Latinović Dragan (Orcid ID: 0000-0003-1859-7346)

Seasonal climate and the onset of the rainy season in Western-Central Brazil simulated by Global Eta Framework model

(Onset of the rainy season in Brazil simulated by GEF model)

Dragan Latinovi [1], Sin Chan Chou[1], Miodrag Ran i [2], Gustavo Sueiro Medeiros[1], André de Arruda Lyra[1]

[1]CPTEC/INPE, Cachoeira Paulista, 12630-000, SP, Brazil
[2]IMSG at EMC/NCEP/NOAA, College Park, 20740, MD, USA

Correspondence to: Dragan Latinovi (dragan.latinovic@cptec.inpe.br)

Key words: GEF, eta model, monsoon onset, rainy season, South America

Abstract. The seasonal cycle of precipitation in tropical South America is determined by the monsoonal system. The transition from dry to wet season occurs in austral spring (September-November, SON) when intense convection from northwestern South America rapidly shifts southward to the southern Amazon Basin and Western-Central Brazil (WCB) in October and further to the Southeast of Brazil in November. This study evaluates ability of the global atmospheric model, Global Eta Framework (GEF), at 25-km horizontal resolution, to simulate the onset of the rainy season in WCB region. The simulations are based on a 5-member ensemble seasonal integrations for the years 2011 and 2013. Evaluation of mean global simulated fields, such as 200-hPa wind, 500-hPa geopotential height, 850-hPa temperature and wind, and MSLP at the surface, for the SON period

indicates high level of agreement with reanalyses and observations, both in spatial distribution and intensity for most of the variables. The variable of the lowest skill is precipitation, which is overestimated over some tropical oceanic regions and underestimated over tropical continental regions, including South America. The onset of the rainy season is determined using methods based on precipitation and outgoing longwave radiation (OLR). The threshold based on simulated precipitation is also calculated as an alternative method for defining monsoon onset. Comparison of the 5-day averaged values (pentads) of precipitation and OLR of all members of the ensemble and the ensemble mean against the observed data shows the ability of GEF to reproduce the typical pattern of transition from dry to wet season in WCB, although most of ensemble members tend to underestimate precipitation and overestimate OLR. The onset date is delayed for few pentads in the model simulations.

1 Introduction

Based on characteristic atmospheric circulation features and their evolution, Zhou and Lau (1998) showed that the monsoonal system also exists over South America. Some other studies related to precipitation and circulation regimes over the continent are documented in Nogués-Paegle et al. (2002) and Vera et al. (2006). Probably the most recognizable characteristic of every monsoon is the seasonal cycle of precipitation. The well defined wet season during austral summer (DJF) and the dry season during austral winter (JJA) represent the typical precipitation regime over tropical South America (Rao et al., 1996; Gan et al., 2004). The period of transition from dry to wet season occurs in austral spring (SON) and it is characterized by a rapid southward shift of the region of intense convection from the Caribbean and northwestern South America to the southern Amazon Basin and Brazilian highlands in October and farther to Southeast Brazil in November. At the onset of the rainy season, the continental subtropical high pressure weakens and the zonal flow changes the intensity and direction (Marengo et al., 2010). Also, the moisture over the Amazon is transported by the low-level jet from the east of the Andes to the central and southeastern Brazil (Rao et al., 1996). The high moisture content and the convergence of the flow in these regions lead to the development of deep convection in WCB. During the austral summer (DJF), the maximum rainfall intensity occurs over most of tropical

South America (Figueroa and Nobre, 1990; Rao and Hada, 1990).

Many studies define the onset and the demise dates of the South American monsoon by applying several criteria. Some criteria are based on OLR (Kousky, 1988; Gonzales et al., 2007; Garcia and Kayano, 2009), some on precipitation (Liebmann and Marengo, 2001; Marengo et al., 2001), while some are based on a combination of wind and precipitation (Gan et al., 2004). The onset and the demise of the rainy season are also evaluated by the monsoon indices based on the dynamical aspects of the atmosphere (Gan et al., 2006), by the Large-Scale Index for South American Monsoon (LISAM) based on combined EOFs (empirical orthogonal functions) of anomalies of precipitation, specific humidity, air temperature, and zonal and meridional winds at 850 hPa (Silva and Carvalho, 2007), or by atmospheric humidity flux over an area recognized as the monsoon core, based on zonal wind reversal and changes in humidity in transition seasons (Raia and Cavalcanti, 2008). Although these methods employ different atmospheric variables, they mostly agree in definition of the mean onset date for South American Monsoon System (SAMS) (Marengo et al., 2010).

Various model simulations of SAMS have been performed at seasonal and climate scales. Simulations from the Coupled Model Intercomparison Project Phase 3 (CMIP3) for the 20th century show difficulties in representing the precipitation amount, and the length of the rainy season in some regions (Bombardi and Carvalho, 2009) or the position and intensity of the Intertropical Convergence Zone (ITCZ) and of the South America Convergence Zone (SACZ) (Seth et al., 2010). Vera and Silvestri (2009) examined simulations of the interannual variability of the South Atlantic convergence zone during summer. They pointed out the necessity for model improvement. Jones and Carvalho (2013) confirmed the improvement of CMIP5 models over CMIP3 models in simulating the SAMS. The ECHAM 4.5 model was evaluated by Liebmann et al. (2007) and demonstrated skill in representing the onset of SAMS during the period between 1976 and 2001. CPTEC-COLA AGCM (Cavalcanti et al., 2002) represented well the large scale characteristics of SAMS in the summer season, but showed precipitation underestimate over the Amazon region and overestimate in the Andes region. An updated version of the CPTEC-COLA AGCM (Cavalcanti and Raia, 2017) represented well the main observed features of the SAMS lifecycle, demonstrating ability to improve precipitation and to capture the change of humidity flux direction. However, simulations also suffered from later onset and

delayed wind reversal. Regional models have also shown to mostly represent well the large-scale features of the SAMS (Chou et al., 2005; Seth et al., 2006; Rocha et al., 2009*).*

The steepness of the Andes, the mountain range that has dominant influence on the weather over South America, represents a challenge for numerical models. The step-wise treatment of the terrain, applied in the regional Eta model, which for years was used for weather forecasting (Saulo et al., 2000; Seluchi et al., 2003), seasonal forecasting (Chou et al., 2005; Bustamante et al., 2012) and climate change studies (Chou et al., 2012, 2014a, 2014b) over Brazil, resolves most of the issues related to terrain following vertical coordinate. Therefore, a global extension of that model, a so-called Global Eta Framework (GEF) is taken for seasonal prediction tests that we are reporting on here. In addition to the vertical coordinate resulting in quasi-horizontal coordinate surfaces, as in the Eta model, GEF is an atmospheric grid-point global model developed in general curvilinear coordinates, capable of running on various squared grids and of avoiding inefficiency and numerical problems originated from the standard longitude-latitude grid. In our tests, GEF was run in an efficient cubed-sphere version, making the model highly scalable and convenient for long-term seasonal prediction experiments.

The objective of this work is to evaluate the capability of the GEF model at a 25-km horizontal resolution, to simulate the seasonal climate and the onset of the rainy season in Western-Central Brazil (WCB) in an ensemble seasonal integration. In the next section, we describe the model, seasonal simulation setup and the dataset used in this study. Section 3 shows the large-scale circulation patterns and Section 4 shows the analysis of pentad averages of rainfall and OLR. We end with summary and conclusions in Section 5.

2 Model specification, methods, and data

The grid-point Eta model (Mesinger et al., 1988; Janjic, 1990; Janjic, 1994; Black, 1994; Chou et al 2002, 2012; Mesinger et al., 2002; Pesquero et al., 2010; Mesinger et al., 2012; Lyra et al., 2017; Mesinger and Veljovic, 2017) is used for weather and climate forecasts over South America at CPTEC/INPE. The model has a conservative, Arakawa type dynamics in the horizontal, and a finite volume representation in vertical (Mesinger and Jovic, 2002). One of the main features of the model is

a step-wise representation of terrain, provided by the so-called "eta" vertical coordinate (Mesinger, 1984) with quasi-horizontal coordinate surfaces. This approach removes the pressure-gradient force errors in areas of steep topography, which is a common error in models with the terrain-following coordinates (e.g. Mesinger and Janjic 1985). In addition, the blocking effect of the eta representation of mountains provides a more realistic flow over large-scale topography and simulation of related precipitation (e.g., Section 2 of Mesinger and Veljovic, 2017), as was shown during many years of operations in the United States of America, Brazil and elsewhere.

Global Eta Framework (GEF) was developed by Zhang and Ran i (2007) as a unique global expansion of the regional Eta model, based on a general curvilinear formalism and capable of running on various rectangular spherical grids. In this study, the model uses a cubed-sphere grid topology, whose symmetry and uniformity enable a highly scalable and efficient computational performance. A specific version of the cubed-sphere used in this study provides an equal-area grid topology (with exception of three grid boxes around the vertices) without angular discontinuities across the edges (Purser and Ran i , 2011; Purser et al., 2014; Ran i et al., 2017). These angular discontinuities characterize the gnomonic cubed-sphere, originally suggested for modeling of the atmosphere by Sadourny (1972).

The physics package of the code includes a choice between two convection schemes, Betts-Miller-Janjic (Betts and Miller, 1986; Janjic, 1994), and Kain-Fritsch (Kain, 2004), and two cloud microphysics schemes, Zhao (Zhao et al., 1997) and Ferrier (Ferrier et al., 2002). The radiation package is developed by GFDL (Geophysical Fluid Dynamics Laboratory), which includes the short-wave radiation scheme of Lacis and Hansen (1974) and the long-wave radiation scheme of Schwarzkopf and Fels (1991), with radiation tendencies calculated every hour and applied at every physics time step. The land–surface transfer processes are parameterized by the Noah scheme (Ek et al., 2003). Monin–Obukhov similarity theory is combined with Paulson stability functions (Paulson, 1970) and applied to the surface layer which includes a molecular viscous sublayer over land according to Zilitinkevich (1995), and over water according to Janjic (1994). Turbulent transports above the surface layer use the Mellor-Yamada 2.5 closure (Mellor and Yamada, 1982; Janjic, 1990).

The step-terrain approach is especially appropriate for the areas where the weather conditions

are strongly affected by steep mountains, such as the Andes Mountains in South America. This and the efficient scalability are among the main reasons for employing GEF in this study. However, GEF still does not employ the "cut-cell" steps, introduced in the regional model in Mesinger et al. (2012), nor the non-hydrostatic acceleration.

The global seasonal forecasts at CPTEC have been produced by an ensemble of the global atmospheric model (AGCM) (Cavalcanti et al., 2002), with the latest results being discussed in Cavalcanti and Raia (2017), an ensemble of coupled ocean-atmosphere model (Siqueira and Nobre, 2006), and an ensemble of the regional Eta model, driven by CPTEC AGCM (Chou et al., 2005; Pilotto et al., 2012). The high computational demand of the spectral model for long-term simulations limits the CPTEC global models to the coarse resolution of about 200 km. The GEF development at CPTEC for seasonal forecasts (Latinovi et al., 2017) is a less computationally demanding alternative for the operational seasonal forecasts at the center.

The model was set up at 25-km horizontal resolution and 38 vertical levels, with model top at 25 hPa, time step 40 s, and so as to use Ferrier cloud microphysics scheme, Kain-Fritsch convection scheme and GFDL radiation package.

This study performs a comparative assessment of simulated and observed seasonal conditions for the trimester September-October-November (SON) of the years 2011 and 2013 with emphasis on the evaluation of the model skill to simulate the onset of the rainy season in the region of WCB (20°S-10°S, 60°W-50°W). For that purpose, the methods based on pentads of precipitation and OLR were adopted, with some modifications needed in view of limitations in information available. The rainy seasons of both selected years ended with extreme floods in the Amazon region (Espinoza et al., 2012, 2014; Marengo et al., 2012; Satyamurty et al., 2013), which motivates the use of these cases in this study. A total of 10 seasonal integrations were performed, for the range of approximately 3.5 months. There were two sets of simulations: one for the period SON of 2011 and another for the period SON of 2013. For each period, 5-member ensemble was constructed by starting the simulations on the days 13, 14, 15, 16, and 17 August of each year. Since the beginning of the analyzed period is 1st of September, approximately 2-3 weeks model spin-up period was left in the case of both years simulations, depending on the member of ensemble. Members of ensemble were constructed using initial conditions

from NCEP reanalyses (Kalnay et al., 1996; Kanamitsu et al., 2002) at 0000 UTC. Sea surface temperature (SST) was updated daily from the observed monthly mean global SST (Reynolds et al., 2002) for each year, while vegetation fraction was also updated daily from monthly mean climatological values. The period analyzed in the Section 3 spans from 1st of September until 30th of November (SON). For the evaluation of the onset of the rainy season in the Section 4, it spans from the pentad 49 until the pentad 66 (29th of August-26th of November). Pentads represent mean values of 5 consecutive days, starting from the 1st of January, where pentad 1 represents the mean value for the days 1st-5th of January, pentad 2 represents the mean value for the days 6th-10th of January, etc., so that one year consists of 73 pentads, as presented in Kousky (1988). The corresponding dates of the pentads used in this study are listed in Table 1. Evaluation of model simulations is carried out by comparing them against corresponding NCEP reanalysis data and CMORPH (CPC MORPHing technique) precipitation data (Joyce et al., 2004).

3 Large-scale circulation patterns

In this section, the large-scale circulation patterns simulated by GEF are discussed, with the focus on South America. Global ensemble mean values of 200-hPa and 850-hPa wind, 500-hPa geopotential height, 850-hPa temperature, mean sea level pressure (MSLP) and precipitation are compared against the corresponding reanalyses and observations of the SON trimester of 2011 and 2013.

Figure 1 shows the mean circulation in the upper troposphere (200 hPa, upper panels), and lower troposphere (850 hPa, lower panels), simulated (left side), and reanalysis verifications (right side), for the two years as indicated on top of the pairs of panels. There are some disagreements with reanalysis in the reproduction of the intensity of the jet streams over North America and over South Pacific, where model tends to simulate weaker winds. On the other hand, the model simulates stronger winds in the western equatorial Indian Ocean and in the eastern equatorial Pacific (Figure 1 a-d). The monsoonal changes at the upper levels, typical of austral spring over South America, are also present in the form of developed anticyclonic circulation, although they are rather displaced in the 2013 case. The

lower-level circulation characteristics that include easterlies over the tropics, the subtropical anticyclonic circulation, the mid-latitude westerlies, and the subpolar lows are reproduced by the model (Figure 1 e-h), although the centers of the subtropical anticyclones and the subpolar lows are slightly displaced toward east. Wind intensity is mostly comparable with reanalysis, except in the western Indian Ocean, where wind speed is overestimated. More pronounced wave-like pattern is simulated in the mid-latitude westerlies in the Southern Hemisphere for both years, but the waves over part of Europe and Asia in 2011 are missing in the simulation. The easterlies over the Atlantic Ocean, near the coast of South America, are more intense in the simulation. The low-level jet east of Andes, which is one of the characteristic features of the South American monsoon, is simulated by the model, although the model simulates a northwest-southeast orientation of the jet whereas the reanalysis has a north-south orientation.

Table 2 shows spatial correlations between the daily mean global simulations and the corresponding reanalyses/observations for SON of 2011 and 2013. The simulated 500-hPa geopotential height and 850-hPa temperature show the best agreement between the model simulations and reanalyses, with spatial correlations of 0.99 and 0.98, respectively, identical for both years. Figure 2 shows 500-hPa geopotential and 850-hPa temperature. Major 500-hPa geopotential height differences are shown in the polar regions and at 5700 and 5800 gpm in the Southern Hemisphere. These geopotential height contours are shifted northwards when compared against reanalysis (Figure 2 a-d). At 850 hPa, the largest temperature error occurs over the Pacific coast of Mexico (Figure 2 e-h), where model overestimates the temperature by about 4°C. Overestimate of 2°C is shown mostly over the equatorial oceanic regions in the eastern Indian Ocean and central Pacific, Atlantic Ocean and over Caribbean Sea. Simulations also overestimate the 850-hPa temperature by about 2°C over western Pacific Ocean in 2013. In contrast, the temperature is mostly underestimated by about 2°C over tropical continental regions such as equatorial Africa, northern Australia, and tropical regions of South America.

Ensemble mean MSLP and precipitation are shown in Figure 3. The model captured the subtropical high-pressure belt, although the pressure was underestimated over south-eastern Pacific Ocean in 2013 (Figure 3 a-d). The surface high-pressure centres of the subtropical anticyclones are displaced eastward especially over the Pacific Ocean in 2011. The subpolar lows, especially in the

Southern Hemisphere, are not so deep as in reanalysis, and the position of the centers are also mainly displaced. In the Amazon region, the simulated 1010-hPa isobar covers a larger area than in reanalysis. Despite these differences, the MSLP field holds the third position in spatial correlation coefficients, when compared with all other evaluated fields (Tab. 2). The spatial correlation for MSLP is 0.89 for the year 2011 and 0.88 for the year 2013. The 200-hPa wind showed the same correlations as MSLP in both years. The 850-hPa wind correlations are 0.86 and 0.85, for 2011 and 2013, respectively. Although spatial correlation is the lowest (0.64 for both years), model precipitation patterns show reasonable agreement with the high-resolution CMORPH observations (Figure 3 e-h). The ITCZ is correctly positioned across the Pacific Ocean and over the Atlantic and Indian Oceans and the Maritime Continent. However, precipitation rate is underestimated over central Pacific, tropical South America, and Africa, and it is overestimated over Central America, Indian Ocean, and the western Pacific. The South Pacific Convergence Zone (SPCZ) that extends from the equatorial west Pacific southeastward across the south Pacific Ocean is correctly positioned. The simulated precipitation rate is also comparable to observed precipitation intensity. Similarly, the precipitation band over South Atlantic that extends from South America also has quantities comparable to the observations. The weak precipitation areas in the Southern Hemisphere mid-latitudes are slightly overestimated by the model, while in the Northern Hemisphere mid-latitudes, the precipitation maxima along and off the eastern coasts of the continents are mostly well represented both in position and intensity. The simulations reproduce the precipitation minima in the subtropics, which correspond to the positions of subtropical highs and the desert regions over the continents along the latitudes of 20°. Model precipitation pattern over South America reproduces the initial phase of the onset of the rainy season which is indicated by the spatial distribution of precipitation, although the intensity of precipitation is clearly underestimated, especially over the Amazon region and the La Plata river basin. Global models generally show dry bias in these two regions (Yin et al., 2012).

4 Analysis of the onset of the rainy season in Western Central Brazil

The definition of the onset of the rainy season in this study is based on precipitation and OLR

for the observed data. Marengo et al. (2001) defined the pentad that represents the onset of the rainy season as the one with daily precipitation greater than 4 mm day^{-1}, preceded by at least 6 out of 8 pentads with daily precipitation less than 3.5 mm day^{-1}, and followed by at least 6 out of 8 pentads with daily precipitation of more than 4.5 mm day^{-1}. The criteria of preceding and subsequent pentads are included due to the fairly noisy character of precipitation and the objective to capture even so the transition from dry to rainy season notwithstanding the appearance of pentads that do not conform to predominant character of pentads they are imbedded in. For example, a pentad with an episode of heavy rain, followed by several pentads with precipitation below the defined threshold, should not be chosen to define the onset.

Another similar method is based on the OLR. Kousky (1988) defines onset as occurring when mean OLR falls below 240 W m^{-2} in a given pentad, provided that 10 out of the 12 previous pentads have OLR above 240 W m^{-2} and 10 out of the 12 subsequent pentads have OLR below 240 W m^{-2}. The WCB region selected for this study (Figure 4) includes the area of maximum precipitation during the rainy season (DJF). The mean annual cycle of circulation is highly related to SAMS, as demonstrated in Gan et al. (2004). They pointed out remarkable seasonality in annual precipitation for the selected region (WCB) and the contrast between the summer and the winter precipitation amounts of more than 900 mm $year^{-1}$ during summer (DJF) and less than 100 mm $year^{-1}$ during winter (JJA) season. This region is also important because it contains the western portion of the Brazilian High Plains together with some rivers that flow into the Amazon and La Plata basins. The WCB area is frequently used in studies related to SAMS to define the onset or demise of the rainy season of South America (Gan et al, 2006; Garcia and Kayano, 2009; Garcia and Kayano, 2011).

Using both methodologies, based on precipitation and on OLR, the onset dates for the years 2011 and 2013 are defined and presented in Figure 5. The two highly correlated curves refer to the NCEP observed OLR data (red line) and the CMORPH precipitation (green line). The x-axis shows pentads from 1 to 73. The y-axis on the left corresponds to precipitation in mm day^{-1} and the inverted y-axis on the right corresponds to OLR in W m^{-2}. Black solid horizontal line represents the thresholds, both for precipitation (4 mm day^{-1}) and OLR (240 W m^{-2}). Both methodologies agree in the indication of the pentad that defines the onset, the pentad 55 (black vertical dashed line) in both years, that

corresponds to the period between 28 September and 2 October. If the demise dates had to be defined, for example, the criterion based on precipitation would give different pentads than using the criterion based on OLR. For the precipitation criterion, they would be the pentad 21 in 2011 and the pentad 22 in 2013 whereas for the OLR criterion, they would be the pentad 22 in 2011 and the pentad 25 in 2013. The first observed peak in precipitation and OLR above the defined threshold in 2011 (pentad 55) indicates the onset, while the first observed peak in 2013 (pentad 50) is followed by 4 consecutive pentads with the values below the threshold. Therefore, it does not qualify to be defined as the onset pentad, which illustrates the importance of the criteria including the preceding and subsequent pentads. Both methods are very sensitive to the definition of threshold, as discussed by Marengo et al. (2001). The OLR threshold value of 230 W m^{-2}, for example, would shift the onset of 2011 probably to a pentad around January of 2012.

Figure 6 shows temporal evolution of 5-day averaged precipitation for each member of the ensemble, referred to as GEF13 to GEF17, the ensemble mean and observation from pentad 49 until pentad 66. These pentads correspond to the period between 29 August and 26 November, approximately the trimester SON. Coefficients r13-r17 are the Pearson correlation coefficients (temporal correlations) for each member of the ensemble and they are a measure of the linear correlation between 2 variables, in this case, between simulated and observed precipitation and between simulated and observed OLR. The names of the members are identified by the suffixes 13-17 which correspond to dates of the initial conditions (13^{th}-17^{th} of August) of each member of the ensemble, while suffix "ens" corresponds to the ensemble mean. The same methods as in Figure 5 cannot be directly applied. The first reason is because the period analyzed here (SON) is shorter than the 24 pentads necessary to apply the OLR method. The second reason is because of the missing information about precipitation before the pentad 49 and after the pentad 66, which could considerably change the onset date. Similarly, if the threshold of 230 W m^{-2} were applied to OLR, there would be change in the 2011 onset, as mentioned in the analysis of Figure 5. The third reason is the definition of threshold for model simulations. For example, the threshold of 4 mm day^{-1} cannot be applied directly because the model underestimates precipitation in South America, as shown in Figure 3. However, it is possible to discuss and assess how the model reproduces the transition from dry to wet season

analyzing each member and ensemble mean and comparing it against observed data.

The observed precipitation data show 6 peaks in precipitation in pentads 52, 55, 58, 62, 64 and 66. The ensemble mean, on the other hand, shows clear peaks in pentads 51, 54, 56, 59, 63 and 65. Most of the ensemble members simulate these peaks, but with different magnitude. Simple comparison of pentads with peak in precipitation indicates that model tends to lead the observed rain episodes, by about 1 pentad in most of the cases. However, the intensity of precipitation is not well simulated. In the first month of the analyzed period (September), before the observed onset in pentad 55, the intensity of precipitation seems reasonably reproduced. An abrupt change in precipitation pattern that represents the onset occurs between September and October. During the same period, the model shows slow increase in precipitation amount, but with underestimate of precipitation. The difference between simulation and observation decreases only in the last 4 pentads of the analyzed period, in November. The correlation coefficients vary between 0.24 and 0.62 among the ensemble members.

The first peak in observed precipitation in 2013 (Figure 6 b) in pentad 50 is almost nonexistent in the model, with barely visible sign of increase, while the second peak, in pentad 52, is more comparable in intensity but it is not clearly defined as a peak by the ensemble precipitation mean. In the period from pentad 51 until pentad 56, the ensemble mean shows constant, almost linear increase, while there are clearly present minima and maxima in the observed data. Simulated peaks in the pentads 56 and 58 correspond to the observed peaks in the pentads 56 and 59. The simulated precipitation, in pentads 59-61, shows the same pattern as the observed precipitation in pentads 60-62, which indicates that the model leads the onset, similarly as in 2011. In the last 5 pentads, although the model improves the simulation of the intensity of precipitation, it seems that the skill in representing the peaks in precipitation decays. Comparison of the correlation coefficients reveals that almost all members of the ensemble, including the ensemble mean, have higher values in 2013. The correlation coefficients varied between 0.41 and 0.73 among the ensemble members. Significant differences occur in the first month of the analyzed period, when the model shows reasonable skill in 2011, however, it mostly fails to simulate some pre-onset maxima in precipitation in 2013. In addition, the ensemble members in 2011 are more mutually comparable in intensity, especially during the first two months of integration, while the members in 2013 are more dispersive, with bigger amplitude in intensity, which

is particularly pronounced in the last month of integration.

With objective to quantitatively define the onset date in the model simulations, the model-relative threshold based on precipitation is also calculated using the modified method of Zeng and Lu (2004). They used a normalized precipitable water index to define globally unified summer monsoon onset and demise dates. Instead of precipitable water, we use precipitation to define a normalized precipitation index (NPI) for the CMORPH observations, similarly as in Geil et al. (2013), with some modifications due to the limitations in information available:

$$NPI = \frac{Pthreshold - Pmin}{Pmax - Pmin}.$$

Pthreshold is the precipitation threshold of 4 mm day^{-1} defined by Marengo et al. (2001) and Pmin and Pmax are the 16-yr climatological values (1998-2013) of the area-averaged minimum and maximum monthly CMORPH precipitation in the WCB region for the period SON. The computed NPI value (0.26) and the values of the area-averaged minimum and maximum monthly precipitation from the 10-member ensemble of the model simulations for the same region and the period SON of 2011 and 2013 are then used to solve the NPI equation for the model-relative precipitation threshold (Pthreshold; mm day^{-1}). The obtained result is 1.91 mm day^{-1} and it is presented with a green dotted horizontal line in the Figure 6, while the red dotted horizontal line represents the threshold of 4 mm day^{-1} for the observed data. If the same method of preceding and subsequent pentads as in Marengo et al. (2001) is applied for the model ensemble mean, the onset by the model will occur at the pentad 58 and 56 for the years 2011 and 2013, respectively.

Figure 7 shows daily mean precipitation over South America, simulated by each ensemble member and ensemble mean, and compared against the corresponding CMORPH observed precipitation. The dates of initial condition of each member of the ensemble (13th-17th of August) are marked at the top of the figure for each year. The black rectangle in the middle of the figure represents the WCB region. All members show underestimate of rain over the Amazon region in 2011. The members 13 and 15 have the lowest amount of precipitation in WCB region, while the member 16 has the highest amount of precipitation in WCB and generally in South America. Nevertheless, the ensemble mean of precipitation, despite the underestimate of precipitation, performs fairly well in the spatial distribution and it is comparable with CMORPH observations. The first two members of

ensemble of 2013, the members 13 and 14, exhibit the best reproduction of precipitation rate when compared with all integrations made for both years. At the same time, the members 15 and 17 exhibit the worst reproduction, especially in the WCB region. As in 2011, the ensemble mean of precipitation shows spatial distribution of reasonable agreement with observations, although with some underestimate.

Figure 8 is similar as Figure 6, only with inverted y-axis and shows OLR. The peaks of the red dashed line represent the minima of observed OLR, due to inverted y-axis. These OLR minima correspond to maxima in precipitation. The model mean OLR follows closely the tendency of decrease of observed OLR values, but without clear signs of minima of OLR during most of the analyzed period, only with weak minima and maxima in the last 6 pentads, which are out of phase (Figure 8 a). Some members of the ensemble, members 13 and 14 and, to some extent 15, show the same pattern in the last 6 pentads, while member 17, for example, reproduces well the pattern of OLR before the onset in pentad 55. The values of OLR are mostly overestimated by the model, especially at the beginning of integration, when the difference reaches almost 80 W m^{-2}. The error reduces with time, reaching the values around 40 W m^{-2} in the middle of integration. Similar values as in observation are shown in the last month of integration. As soon as the model starts to produce rain, that error in OLR decreases. From the onset until the end of integration, the model shows some skill as it simulates the minimum at the pentad 61, although it still overestimates OLR by a relatively constant difference of about 40-50 W m^{-2}. Correlations vary between 0.53 and 0.85.

The observed precipitation and OLR are highly inversely correlated variables (Figure 9). Each maximum in precipitation (green line) corresponds to a minimum in OLR (red line) and vice versa. Therefore, the temporal correlation between the two variables is negative, such as -0.97 for 2011 (Figure 9 b) and -0.94 for 2013 (Figure 9 d), for the same period as in Figure 6 and Figure 8. Although the ensemble mean precipitation and OLR simulated by the model are inversely correlated, the values of correlation coefficients -0.69 for 2011 (Figure 9 a) and -0.76 for 2013 (Figure 9 c) are lower than the correlation of the observations.

Time-longitude daily mean precipitation, averaged over 20°S-10°S for the period SON 2011 and 2013, is shown in Figure 10. The model simulates some pre-onset episodes of rain in WCB region

in September, with the first intense continuous precipitation occurring in the period 23-28 September (approximately pentad 54), while in the observations the onset is identified in the period 26 September-2 October (approximately pentad 55). Lower charts show the ensemble mean simulated by the model for 2013 on the left and the observed data on the right. The pattern is somewhat similar to that of 2011, with the difference that the model produces little rain in the first 20 days of September in 2013. Some weak rain is only simulated at the beginning of the last 10 days of September. More intense rain is simulated only in the eastern part of the WCB region in the period 1-6 October (approximately pentad 56). Observed data show some rainy episodes in September with more intense continuous rain occurring in the period 28 September-2 October (approximately pentad 55). Precipitation is notably more intense in observations than in simulations for both years.

5 Summary and conclusions

The main objective of this study was to assess the skill of GEF for seasonal simulations and to evaluate model capability to simulate the onset of the rainy season in the WCB region. Ensemble seasonal forecasts and observations of years 2011 and 2013 were used to this end. A comparative analysis was performed of simulations and observations or reanalyses of global mean fields for the period SON of both years, in the first part of this work. Some preliminary results with this version of the model were shown in Latinovi et al. (2017), where the ability of GEF to perform simulations with increased horizontal resolution and upgraded version of cubed-sphere and its stability in long-term seasonal integrations were confirmed. The results shown here show high level of spatial correlation between the model simulations and the reanalyses for almost all analyzed variables, with correlations of 5 out of 6 variables varying from 0.85 to 0.99. The magnitude of most of the variables is also well represented by the model, although with some local differences. Variables from different levels are evaluated: for the upper-troposphere, the 200-hPa wind, for the mid-troposphere, the 500-hPa geopotential height, and for the lower-troposphere, the 850-hPa temperature and wind, and at the surface, MSLP. These variables represent the dynamical part of the model and demonstrate satisfactory skill for both years in seasonal integration for the period SON. Although precipitation is the variable of

lowest simulation skill, the model reproduces reasonably well the spatial distribution of precipitation, with spatial correlation of 0.64, in both years. Precipitation over some tropical oceanic regions is mostly overestimated and over tropical continental regions is mostly underestimated. The second part of our study presents analyses of the onset of the rainy season in WCB region based on the methods that employ precipitation and OLR. The onset defined from observations occurs in the pentad 55 in both years. The simulations show underestimate in precipitation and overestimate in OLR, therefore, the thresholds from observations are not applied in the model outputs of these variables. Limitation is also present in the length of analyzed period where the criteria of preceding and subsequent pentads, applied in both methods could not be applied directly. Still, comparative assessment of temporal evolution of the 5-day averaged simulated and observed precipitation through the period SON demonstrates that the model ensemble mean possesses satisfactory skill in predicting maxima of precipitation even toward the end of the observed period, with errors of around 1 pentad when compared with observed data. Simulated precipitation shows continuous increase along the period rather than an abrupt change in regime typical of transition from dry to wet season. On the other hand, the intensity was comparable with observations in the first and in the last month of the period. Some ensemble members, however, show some signs of sudden change in precipitation intensity near the observed onset pentad, but with underestimated values. The temporal correlations of 0.58 and 0.61 for the years 2011 and 2013, respectively are considered satisfactory. In addition to comparative assessment, the model-related threshold is explicitly defined and it indicates 1-3 pentads later onset then in observed data.

In comparison with precipitation, members of the ensemble of OLR generally show higher linear temporal correlation with observations, with ensemble mean value of 0.81 for 2011 and 0.69 for 2013. The extreme values in OLR are to some extent simulated by several members of the ensemble, but they mostly disagree in the timing of these minima or maxima, therefore the ensemble mean results in smooth line, with no clear peaks. On the other hand, the OLR simulations generally represent well the trend, which is similar to the observations. In addition, OLR is clearly overestimated in 2013. The high temporal correlation between the ensemble mean precipitation and the ensemble mean OLR indicates a reasonable agreement of these two variables, although with moderately lower correlations

than in observation.

The ability of the model to simulate the onset of the rainy season in WCB is illustrated in Figure 10, which shows the time-longitude section of daily averaged precipitation over the latitudes 20°S-10°S. The simulation clearly shows the transition of precipitation regime from dry to wet, approximately at the end of September to beginning of October, which differs from observation by a couple of days. Simulation of precipitation pattern changes and more intense precipitation starts to occur after that date, although still significantly less intense than observation.

The underestimate of the precipitation rate over tropical continental regions, particularly over South America, remains one of the main issues of the model. Although the model simulates reasonably well the formation of the main features of the SAMS, some discrepancies are noted and they indicate some weaknesses of the model. Without properly simulated enhanced convective activity in the Amazon region, which typically starts in SON, and intense latent heat release in the area of heavy precipitation, the model is not able to reproduce well the large-scale patterns. The Bolivian High, explained as response to local diabatic heating in the Amazon region (Lenters and Cook, 1997), is not sufficiently developed in the model. This weakness affects the circulation pattern in the region, and moisture flux from the Amazon toward southeast Brazil, which is an important mechanism for the maintenance of SACZ. Therefore, the further improvements and adjustments of the convection scheme are necessary for better simulations. However, the recently implemented and tested radiation scheme, RRTMG (Rapid Radiative Transfer Model for GCMs), which we did not use, produced downward surface shortwave radiation fluxes closer to observations and reduced the systematic positive bias found in the regional Eta model (de Andrade Campos et al., 2017). It demonstrated better performance in most of evaluated variables, especially in clear-sky conditions. Once implemented in GEF, it could potentially bring benefits in the representation of radiation and precipitation as well. The computational efficiency of GEF shown by Zhang and Ran i (2007) and the results presented in this study suggest that continuous efforts in development of the model can give significant contribution to the improvement of the seasonal forecasts at CPTEC.

Competing interests

The authors declare that they have no conflict of interest.

Acknowledgements

This work is supported by scholarships of the CAPES foundation of Ministry of Education in Brazil and the Brazilian National Council of Technological and Scientific Development (CNPq) No: 140952/2015-2 and 306757/2017-6.

References

Betts AK, Miller MJ.1986. A new convective adjustment scheme. Part II: single column tests using GATE wave, BOMEX, ATEX and arctic air-mass data sets. *Q. J. R. Meteorol. Soc.* **112**: 693–709. doi:10.1002/qj.49711247308.

Black TL. 1994. The new NMC mesoscale Eta model: Description and forecast examples. *Weather and Forecasting* **9**: 265–278.

Bombardi RJ, Carvalho LMV. 2009. IPCC global coupled model simulations of the South America monsoon system. *Clim. Dyn.* **33**: 893–916.

Bonatti JP. 1996. Modelo de Circulação Geral Atmosférico do CPTEC. *Climanálise* Edição Comemorativa de 10 anos, Instituto Nacional de Pesquisas Espaciais, http://climanalise.cptec.inpe.br/~rclimanl/boletim/cliesp10a/bonatti.html (last access: 26 November 2017).

Bustamante JF, Chou SC, Sueiro GM. 2012. Climatologia das previsões sazonais do modelo Eta sobre a América do Sul. *Anais do XVII Congresso Brasileiro de Meteorologia*. Gramado, RS. ISBN: 978-85-63273-15-

Cavalcanti IFA, Raia A. 2017. Lifecycle of South American Monsoon System simulated by CPTEC/INPE AGCM. *Int. J. Climatol.* **37**: S1 878–896. doi: 10.1002/joc.5044.

Cavalcanti IFA, Marengo JA, Satyamurty P, Trosnikov I, Bonatti J, Nobre CA, D'Almeida C, Sampaio G, Castro CAC, Camargo H, Sanches MB. 2002. Global climatological features in a simulation using CPTEC/COLA AGCM. *J. Clim.* **15**: 2965–2988.

Chou SC, Bustamante JF, Gomes JL. 2005. Evaluation of Eta Model seasonal precipitation forecasts

over South America, *Nonlin. Processes Geophys.* **12**: 537–555. https://doi.org/10.5194/npg-12-537-2005.

Chou SC, Nunes AMB, Cavalcanti IFA. 2000. Extended range forecasts over South America using the regional Eta model. *J. Geophys. Res*. **105**: 10147–10160.

Chou SC, Marengo JA, Lyra A, Sueiro G, Pesquero J, Alves LM, Kay G, Betts R, Chagas D, Gomes JL, Bustamante J, Tavares P. 2012. Downscaling of South America present climate driven by 4-member HadCM3 runs. *Clim. Dynam.* **38**: 635–653. https://doi.org/10.1007/s00382-011-1002-8.

Chou SC, Lyra A, Mourão C, Dereczynski C, Pilotto I, Gomes J, Bustamante J, Tavares P, Silva A, Rodrigues D, Campos D, Chagas D, Sueiro G, Siqueira G, Nobre P, Marengo J. 2014a. Evaluation of the Eta Simulations Nested in Three Global Climate Models. *American Journal of Climate Change*. **3**: 438–454.

Chou SC, Lyra A, Mourão C, Dereczynski C, Pilotto I, Gomes J, Bustamante J, Tavares P, Silva A, Rodrigues D, Campos D, Chagas D, Sueiro G, Siqueira G, Marengo J. 2014b. Assessment of Climate Change over South America under RCP 4.5 and 8.5 Downscaling Scenarios. *American Journal of Climate Change.* **3**: 512–527.

Da Rocha RP, Morales CA, Cuandra SV, Ambrizzi T. 2009. RegCM3 assessment over South America: Summer seasonal climatology and precipitation diurnal cycle. *Journal of Geophysical Research* **114**: D10108, doi: 10.1029/2008JD010212.

De Andrade Campos D, Chou SC, Spyrou C, Chagas JCS, Bottino MJ. 2018. Eta model simulations using two radiation schemes in clear-sky conditions. *Meteorology and Atmospheric Physics* **130**: 39. https://doi.org/10.1007/s00703-017-0500-6.

Ek M, Mitchell KE, Lin Y, Rogers E, Grunmann P, Koren V, Gayno G, Tarpley JD. 2003. Implementation of Noah land-surface model advances in the NCEP operational mesoscale Eta model. *J. Geophys. Res.* **108**: 8851. doi:10.1029/2002JD003296.

Espinoza JC, Marengo JA, Ronchail J, Carpio JM, Flores LN, Guyot JL. 2014. The extreme 2014 flood in south-western Amazon basin: the role of tropical-subtropical South Atlantic SST gradient. *Environmental Research Letters.* **9**: 124007. https://doi.org/10.1088/1748-9326/9/12/124007

Espinoza JC, Ronchail J, Frappart F, Lavado W, Santini W, Guyot JL. 2012. The Major Floods in the Amazonas River and Tributaries (Western Amazon Basin) during the 1970-2012 Period: A Focus on the 2012 Flood. *Journal of Hydrology*. **14**: 1000-1008.

Ferrier BS, Jin Y, Lin Y, Black T, Rogers E, DiMego G. 2002. Implementation of a new grid-scale cloud and precipitation scheme in the NCEP Eta Model. In: 19th conference on weather analysis and forecasting/15th conference on numerical weather prediction, San Antonio. *Am. Meteorol. Soc.*: 280–283.

Figueroa SN, Nobre CA. 1990. Precipitation distribution over central and western tropical South America. *Climanálise* **5**: 25–40.

Figueroa SN, Bonatti JP, Kubota PY, Grell GA, Morrison H, Barros SRM, Fernandez JPR, Ramirez E, Siqueira L, Luzia G, Silva J, Silva JR, Pendaharkar J, Capistrano VB, Alvim DS, Enoré DP, Diniz FLR, Satyamurti P, Cavalcanti IFA, Nobre P, Barbosa HMJ, Mendes CL, Panetta J. 2016. The Brazilian global atmospheric model (BAM): performance for tropical rainfall forecasting and sensitivity to convective scheme and horizontal resolution. *Weather Forecast.* **31**: 1547–1572.

Gan MA, Kousky VE, Ropelewski CF. 2004. The South America monsoon circulation and its relationship to rainfall over West-Central Brazil. *Journal of Climate* **17**: 47–66.

Gan MA, Rao VB, Moscati MCL. 2006. South American monsoon indices. *Atmospheric Science Letters* **6**: 219–223.

Garcia SR, Kayano MT. 2009. Determination of the onset dates of the rainy season in central Amazon with equatorially antisymmetric outgoing longwave radiation. *Theoretical and Applied Climatology* **97**: 361–372.

Garcia SR, Kayano MT. 2011. Moisture and heat budgets associated with the South American monsoon system and the Atlantic ITCZ. *Int. J. Climatol.* **31**: 2154–2167.

Geil KL, Serra YL, Zeng X. 2013. Assessment of CMIP5 model simulations of the North American Monsoon System, *Journal of Climate*, **26**(22):8787-8801

Gonzalez M, Vera CS, Liebmann B, Marengo J, Kousky V, Allured D. 2007. The nature of the rainfall onset over central South America. *Atmosfera* **20**: 377–394.

Janjic ZI. 1990. The step-mountain coordinate: physical package. *Mon. Weather Rev.* **118**: 1429–1443.

Janjic ZI. 1994. The step-mountain eta coordinate model: Further developments of the convection, viscous sublayer, and turbulence closure schemes. *Mon. Weather Rev.* **122**: 927–945.

Jones C, Carvalho LMV. 2013. Climate change in the South American monsoon system: present climate and CMIP5 projections. *J. Clim.* **26**: 6660–6678.

Joyce RJ, Janowiak JE, Arkin PA, Xie P. 2004. CMORPH: A Method That Produces Global Precipitation Estimates From Data At High Spatial And Temporal Resolution. *J. Hydrometeor.* **5**: 487-503.

Kain JS. 2004. The Kain−Fritsch convective parameterization: An update. *J. Appl. Meteor*. **43**: 170−181.

Kalnay E, Kanamitsu M, Kistler R, Collins W, Deaven D, Gandin L, Iredell M, Saha S, White G, Woollen J, Zhu Y, Leetmaa A, Reynolds R, Chelliah M, Ebisuzaki W, Higgins W, Janowiak J, Mo KC, Ropelewski C, Wang J, Jenne R, Joseph D. 1996. The NCEP/NCAR 40-year reanalysis project. *Bull. Amer. Meteor. Soc.* **77**: 437-470.

Kanamitsu M, Ebisuzaki W, Woollen J, Yang S-K, Hnilo JJ, Fiorino M, Potter GL. 2002. NCEP-DOE AMIP-II Reanalysis (R-2). *Bulletin of the American Meteorological Society*: 1631-1643.

Kousky VE. 1988. Pentad outgoing longwave radiation climatology for the South American sector. *Revista Brasileira de Meteorologia* **3**: 217–231.

Lacis AA, Hansen JE. 1974. A parameterization of the absorption of solar radiation in the Earth's atmosphere. *J. Atmos. Sci.* **31**: 118-133.

Latinovi D, Chou SC, Ran i M. 2017. Seasonal range test run with Global Eta Framework. *Adv. Sci. Res.* **14**: 247-251. https://doi.org/10.5194/asr-14-247-2017.

Lenters JD, Cook KH. 1997. On the origin of the Bolivin High and related circulation features of the South America climate. *Journal of the Atmospheric Sciences*, **54**: 656–677.

Liebmann B, Marengo J. 2001. Interannual variability of the rainy season and rainfall in the Brazilian Amazon Basin. *Journal of Climate* **14**: 4308–4318.

Liebmann B, Camargo SJ, Seth A, Marengo JA, Carvalho LM, Allured D, Fu R, Vera CS. 2007. Onset and end of the rainy season in South America in observations and the ECHAM 4.5 atmospheric general circulation model. *J. Clim.* **20**: 2037–2050.

Lyra A, Tavares P, Chou SC, Sueiro G, Dereczynski C, Sondermann M, Silva A, Marengo J, Giarolla A. 2017. Climate change projections over three metropolitan regions in Southeast Brazil using the non-hydrostatic Eta regional climate model at 5-km resolution. *Theor. Appl. Climatol.* https://doi.org/10.1007/s00704-017-2067-z.

Marengo JA, Tomasella J, Soares WR. 2012. Extreme Climate Events in the Amazon Basin. *Theoretical and Applied Climatology*. **107**: 73-85. http://dx.doi.org/10.1007/s00704-011-0465-1

Marengo J, Liebmann B, Kousky VE, Filizola N, Wainer I. 2001. On the onset and end of the rainy season in the Brazilian Amazon Basin. *Journal of Climate* **14**: 833–852.

Marengo JA, Liebmann B, Grimm AM, Misra V, Silva Dias PL, Cavalcanti IFA, Carvalho LMV, Berbery EH, Ambrizzi T, Vera CS, Saulo AC, Nogues-Paegle J, Zipser E, Seth A, Alves LM. 2012. Recent developments on the South American monsoon system. *Int. J. Climatol.* **32**: 1–21. doi:10.1002/joc.2254.

McGregor JL. 1996. Semi-Lagrangian advection on conformal-cubic grids. *Mon. Weather Rev.* **124**: 1311–1322.

Mellor GL, Yamada T. 1982. Development of a turbulence closure model for geophysical fluid problems. *Rev. Geophys. Space Phys.* **20**: 851–875.

Mesinger FA. 1984. Blocking technique for representation of mountains in atmospheric models. Riv. Meteor. *Aeronáutica* **44**: 195–202.

Mesinger F, Janjic ZI. 1985. Problems and numerical methods of the incorporation of mountains in atmospheric models. *Large-Scale Computations in Fluid Mechanics.* Eds: Engquist BE, Osher S, Somerville CJ, Lectures in Applied Mathematics **22**: 81-120.

Mesinger F, Jovic D. 2002. The Eta slope adjustment: Contender for an optimal steepening in a piecewise-linear advection scheme? Comparison tests. NOAA/NCEP Office Note 439 available at: http://www.emc.ncep.noaa.gov/officenotes/newernotes/on439.pdf (last access: 26 November 2017).

Mesinger F, Veljovic K. 2017. Eta vs sigma: Review of past results, Gallus–Klemp test, and large-scale wind skill in ensemble experiments. *Meteorol. Atmos. Phys.* https://doi.org/10.1007/s00703-016-0496-3.

Mesinger F, Janjic ZI, Ni kovi S, Gavrilov D, Deaven DG. 1988. The step mountain coordinate: Model description and performance for cases of Alpine cyclogenesis and for a case of an Appalachian redevelopment. *Mon. Weather Rev.* **116**: 1493–1518.

Mesinger F, Chou SC, Gomes JL, Jovic D, Bastos P, Bustamante JF, Lazic L, Lyra AA, Morelli S, Ristic I, Veljovic K. 2012. An upgraded version of the Eta model. *Meteorol. Atmos. Phys.* **116**: 63–79. https://doi.org/10.1007/s00703-012-0182-z.

Nogués-Paegle J, Mechoso CR, Fu R, Berbery EH, Chao WC, Chen TC, Cook K, Diaz AF, Enfield D, Ferreira R, Grimm AM, Kousky V, Liebmann B, Marengo J, Mo K, Neelin JD, Paegle J, Robertson AW, Seth A, Vera CS, Zhou J. 2002. Progress in Pan American CLIVAR research: Understanding the South American monsoon. *Meteorologica*, **27**: 3-32.

Paulson CA. 1970. The mathematical representation of wind speed and temperature profiles in the unstable atmospheric surface layer. *J. Appl. Meteor.* **9**: 857–861.

Pesquero JF, Chou SC, Nobre CA, Marengo JA. 2010. Climate downscaling over South America for 1961–1970 using the Eta Model. *Theor. Appl. Climatol.* **99**: 75–93. https://doi.org/10.1007/s00704-009-0123-z.

Purser RJ, Ran i M. 1998. Smooth quasi-homogeneous gridding of the sphere. *Q. J. R. Meteorol. Soc.* **124**: 637–647.

Purser RJ, Ran i M. 2011. A standardized procedure for the derivation of smooth and partially overset grids on the sphere, associated with polyhedra that admit regular griddings of their surfaces. Part I: Mathematical principles of classification and construction. NOAA/NCEP Office Note 467, available at: http://www.emc.ncep.noaa.gov/officenotes/newernotes/on467.pdf (last access: 26 November 2017).

Purser RJ, Ran i M, Jovi D, Latinovi D. 2014. Two strategies for the mitigation of coordinate singularities of a spherical polyhedral grid, Presentation from 2014 PDEs workshop, Boulder,

CO, USA, available at: http://www.cgd.ucar.edu/events/20140407/Presentations-Posters/Purser.pdf (last access: 26 November 2017).

Raia A, Cavalcanti IFA. 2008. The Life Cycle of the South American Monsoon System. *J. Clim.* **21**: 6227–6246.

Ran i M, Purser RJ, Mesinger F. 1996. A global shallow-water model using an expanded spherical cube: gnomonic versus conformal coordinates. *Q. J. R. Meteorol.* Soc. **122**: 959–982.

Ran i M, Purser RJ, Jovi D, Vasi R, Black T. 2017. A nonhydrostatic multiscale model on the uniform Jacobian cubed sphere, *Mon.Weather Rev.* https://doi.org/10.1175/MWR-D-16-0178.1.

Rao VB, Hada K. 1990. Characteristics of rainfall over Brazil: Annual variations and connections with the Southern Oscillation. *Theor. Appl. Climatol.* **42**: 81–92.

Rao GV, Cavalcanti I, Hada K. 1996. Annual variations of rainfall over Brazil and water vapor characteristics of South America. *J. Geophys. Res.* **101** (D21): 26539–26551, doi:10.1029/96JD01936.

Ronchi C, Iacono R, Paolucci R. 1996. The "cubed sphere": a new method for the solution of partial differential equations in spherical geometry. *J. Comput. Phys.* **124**: 93–114.

Sadourny R. 1972. Conservative finite-differencing approximations of the primitive equations on quasi-uniform spherical grids. *Mon. Weather Rev.* **22**: 1107–1115.

Satyamurty P, da Costa CP, Manzi AO, Candido LA. 2013. A Quick Look at the 2012 Record Flood in the Amazon Basin. *Geography Research Letter*. **40**: 1-6. http://dx.doi.org/10.1002/grl.50245

Saulo C, Nicolini M, Chou SC. 2000. Model characterization of the South American low-level flow during the 1997-1998 spring-summer season. *Climate Dynamics*. **16**, 867–881.

Schwarzkopf MD, Fels SB. 1991. The simplified exchange method revisited: an accurate, rapid method for computation of infrared cooling rates and fluxes. *J. Geophys. Res.* **96**: 9075–9096.

Seluchi ME, Norte F, Satyamurty P, Chou SC. 2003. Analysis of three situations of foehn effect over the Andes. *Weather and Forecasting*. **18**, 481-501.

Seth A, Rojas M, Rauscher S. 2010. CMIP3 projected changes in the annual cycle of the South American Monsoon. *Clim. Change* **98**: 331–357.

Seth A, Rauscher S, Camargo S, Qian J-H, Pal J. 2006. RegCM regional climatologies for South America using reanalysis and ECHAM model global driving fields. *Climate Dynamics (2007)* **28**: 461. DOI:10.1007/s00382-006-0191-z.

Silva AE, Carvalho LMV. 2007. Large-scale index for South America Monsoon (LISAM). *Atmospheric Science Letters* **08**: 51–57.

Siqueira L, Nobre P. 2006. Tropical Atlantic sea surface temperature and heat flux simulations in a coupled GCM. *Geophys. Res. Lett.* **33**: L15708. https://doi.org/10.1029/2006GL026528.

Vera C, Silvestri G. 2009. Precipitation interannual variability in South America from the WCRP-CMIP3 multi-model dataset. *Clim. Dyn.* **32**: 1003–1014. doi: 10.1007/s00382-009-0534-7.

Vera C, Higgins W, Amador J, Ambrizzi T, Garreaud R, Gochis D, Lettenmaier DD, Marengo J, Mechoso CR, Paegle JN, Silva Dias PL, Zhang C. 2006. A unified view of the American Monsoon Systems. *Journal of Climate* **19**: 4977–5000.

Yin L, Fu R, Shevliakova E, Dickinson RE. 2013. How well can CMIP5 simulate precipitation and its controlling processes over tropical South America?. *Climate Dynamics* **41** (11-12): 3127–3143.

Zeng X, Lu E. 2004. Globally unified monsoon onset and retreat indexes. *Journal of Climate*, **17**, 2241–2248.

Zhang H, Ran i M. 2007. A global Eta model on quasi-uniform grids. *Q. J. Roy. Meteorol. Soc.* **133**: 517–528.

Zhao Q, Black TL, BaldwinME. 1997. Implementation of the cloud prediction scheme in the Eta Model at NCEP. *Wea. Forecasting* **12**: 697–712.

Zhou J, Lau WK-M. 2001. Principal modes of interannual and decadal variability of summer rainfall over South America. *International Journal of Climatology* **21**: 1623–1644.

Zilitinkevich SS. 1995. Non-local turbulent transport: Pollution dispersion aspects of coherent structure of convective flows. Power H, Moussiopoulos N, Brebbia CA (eds) Air pollution III. Air pollution theory and simulation, vol I. Computational Mechanics Publications, Southampton, 53–60.

Captions

Figure 1: September to November (SON) 2011 and 2013 ensemble mean of 200-hPa and 850-hPa winds (m s^{-1}), GEF simulations (on the left) and NCEP reanalyses (on the right). Wind speed is shaded and direction is shown by streamlines. Top panel refers to 200-hPa wind (m s^{-1}) in 2011, the second panel shows 200-hPa wind (m s^{-1}) in 2013, the third panel shows 850-hPa wind (m s^{-1}) in 2011 and the bottom panel shows the 850-hPa winds (m s^{-1}) in 2013.

Figure 2: September to November (SON) 2011 and 2013 ensemble mean 500-hPa geopotential height (gpm) (contour) and 850-hPa temperature (°C) (shaded) simulated by GEF (on the left) and the corresponding variables from NCEP reanalyses (on the right). Top row refers to 500-hPa geopotential height (gpm) in 2011, the second row shows 500-hPa geopotential height (gpm) in 2013, the third row shows 850-hPa temperature (°C) in 2011 and the bottom row shows 850-hPa temperature (°C) in 2013.

Figure 3: 2011 and 2013 SON global ensemble mean MSLP (hPa) (contour) and precipitation (mm day^{-1}) (shaded); GEF simulations (on the left) and NCEP reanalyses and observed precipitation (mm day^{-1}) from CMORPH (on the right). Top row refers to MSLP (hPa) in 2011, the second row refers to MSLP (hPa) in 2013, the third row shows precipitation (mm day^{-1}) in 2011 and the bottom row shows precipitation (mm day^{-1}) in 2013.

Figure 4: Study area to define the rainy season onset: Western-Central Brazil (WCB), 10°S–20°S/60°W–50°W.

Figure 5: The onset of the rainy season in WCB for the years (a) 2011 and (b) 2013. 5-day averaged time series of OLR (W m^{-2}) are presented by the red curve and precipitation (mm day^{-1}) by the green curve. The solid horizontal line refers to the thresholds defined for both methods and the vertical dashed line defines the onset pentads.

Figure 6: 5-day averaged time series of precipitation (mm day^{-1}) of all members of the ensemble, ensemble mean and observation in WCB and temporal correlation coefficients for the period 29 August-26 November (pentads 49-66) of the years (a) 2011 and (b) 2013. Red dotted horizontal lines

represent the threshold for the observed data, while the green dotted horizontal lines represent the model-relative threshold.

Figure 7: SON daily mean precipitation (mm day^{-1}) over South America. The members of the ensemble for the year 2011 are in the top row (a) and for the year 2013 in the middle row (b). Comparison of the ensemble mean simulated and CMORPH observed precipitation (mm day^{-1}) for 2011 is in the bottom left row (c) and for 2013 in the bottom right row (d). The WCB region is identified by the black rectangle. The numbers 13-17 above figures are the dates of the initial conditions in August 2011 and 2013 for each ensemble member.

Figure 8: 5-day averaged time series of OLR (W m^{-2}) of all members of ensemble, ensemble mean and observation in WCB and temporal correlation coefficients for the period 29 August-26 November (pentads 49-66) of the years (a) 2011 and (b) 2013.

Figure 9: Comparison between simulated and observed 5-day averaged time series of precipitation (mm day^{-1}) (green curve) and OLR (W m^{-2}) (red curve) in WCB for the years 2011 (top row) and 2013 (bottom row). The temporal correlation between precipitation and OLR for the period 9 August-26 November (pentads 49-66) is plotted. The negative values show the inverse correlation between precipitation and OLR.

Figure 10: Time-longitude daily precipitation (mm day^{-1}) averaged over 20°S–10°S for the period 29 August-26 November (pentads 49-66) of 2011 (top row) and 2013 (bottom row). Simulated precipitation (mm day^{-1}) is on the left ((a) and (c)) and observed precipitation is on the right ((b) and (d)).

Table 1: Pentad numbers and corresponding dates for the pentads 49-66.

Table 2: Spatial correlations between mean global simulations and CMORPH observations for precipitation (mm day^{-1}) and the NCEP reanalysis for the remaining variables entered, for SON of 2011 and 2013.

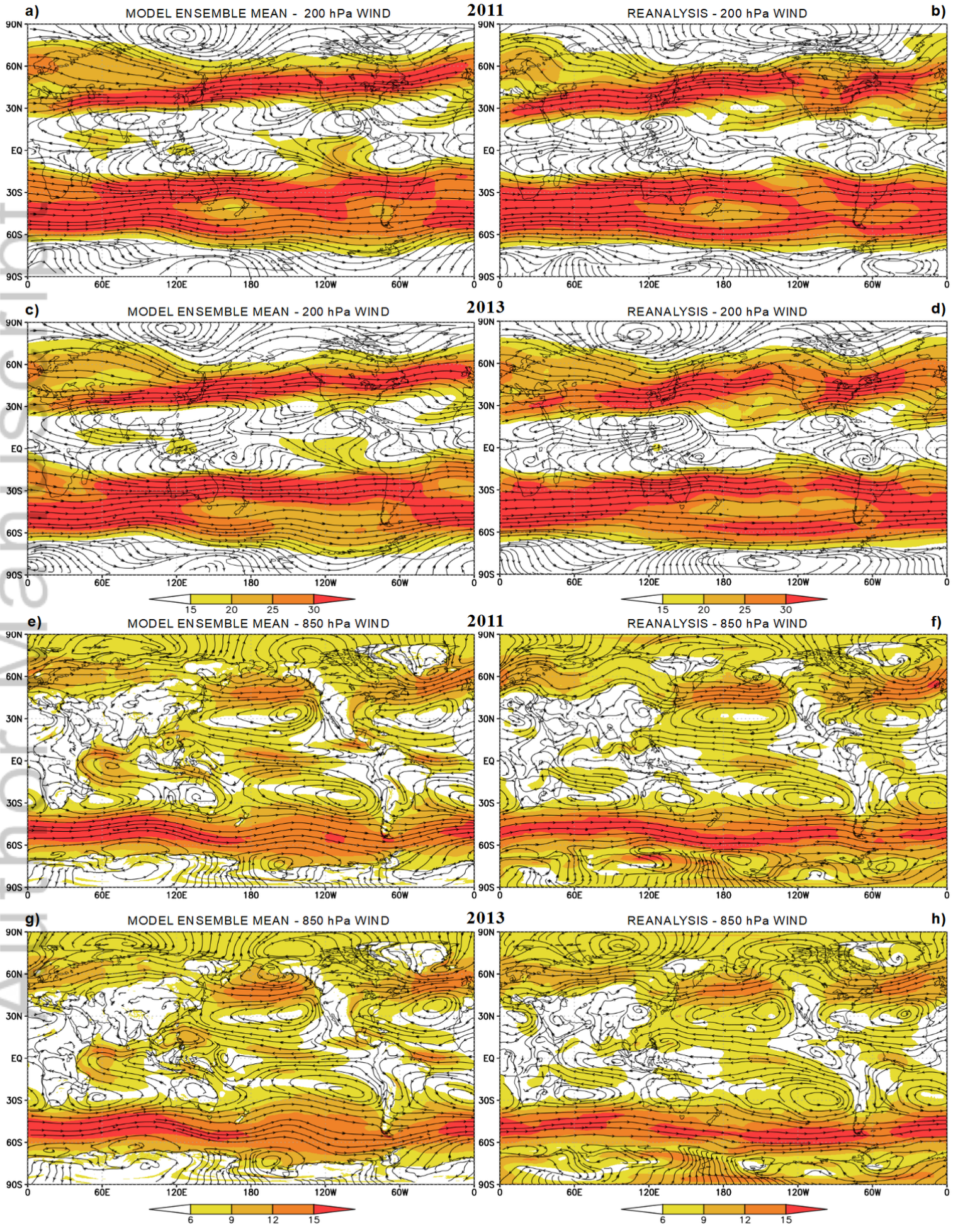

Dragan_Latinovic_figure_1.tif

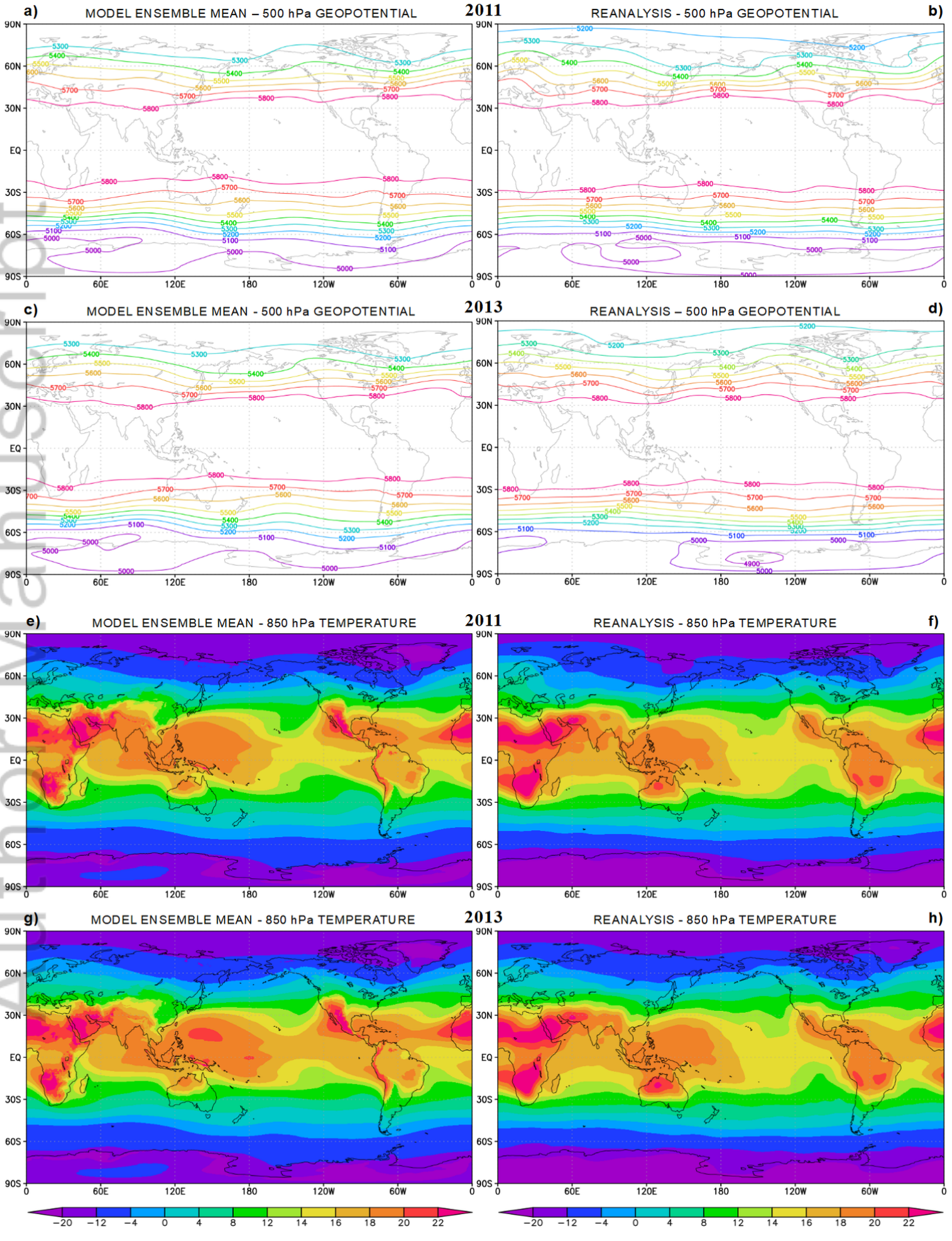

Dragan_Latinovic_figure_2.tif

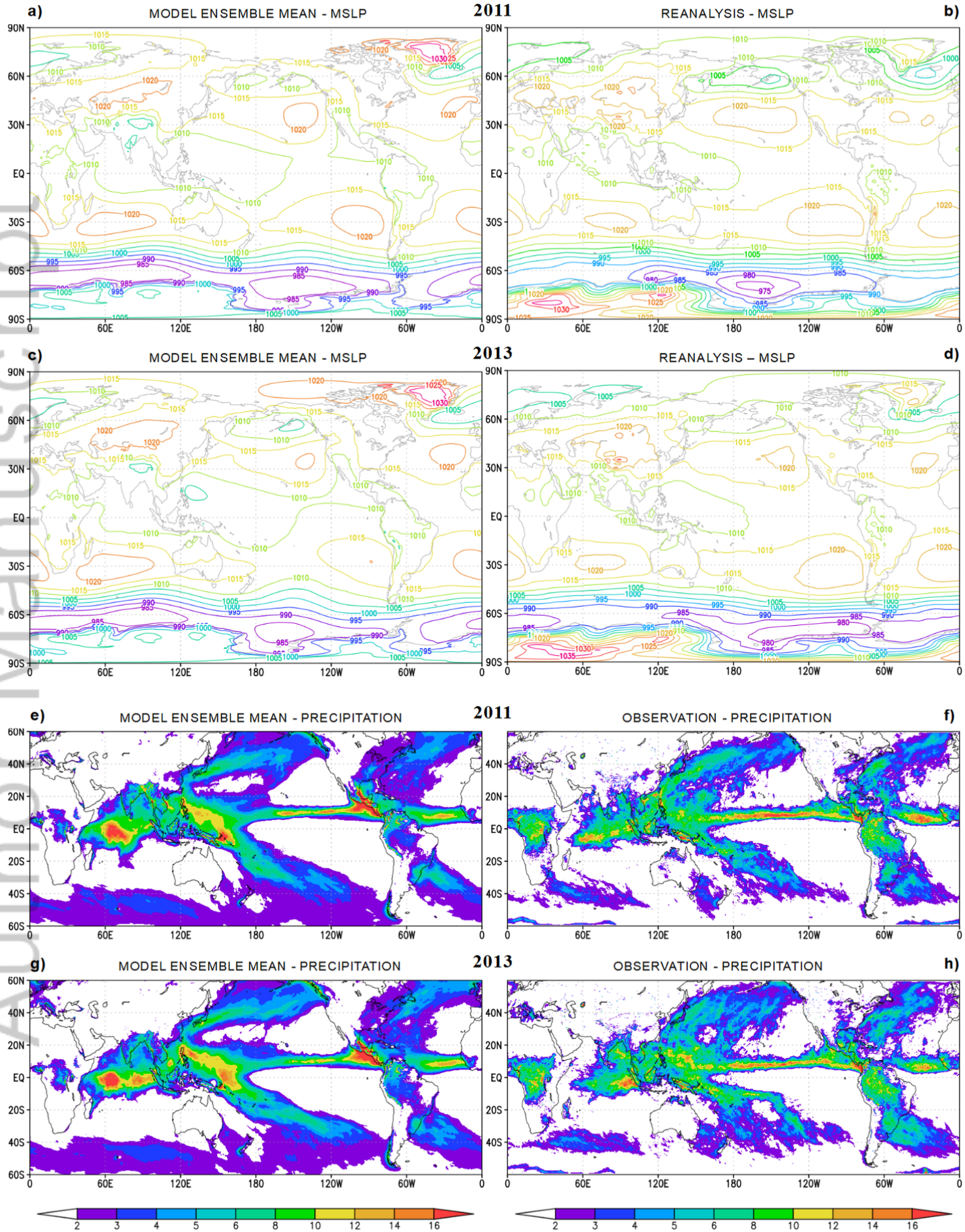

Dragan_Latinovic_figure_3_new.tif

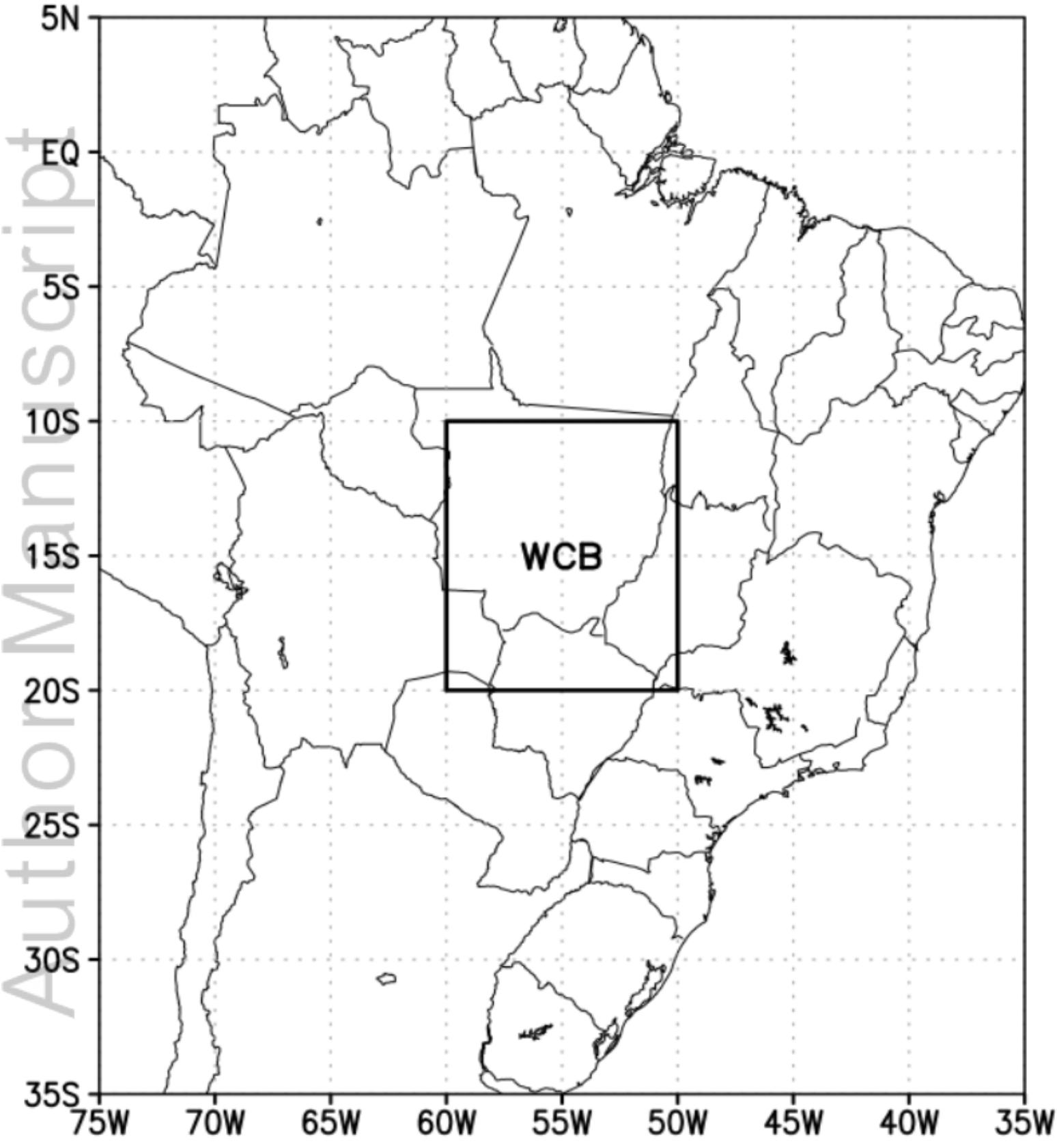

Dragan_Latinovic_figure_4.tif

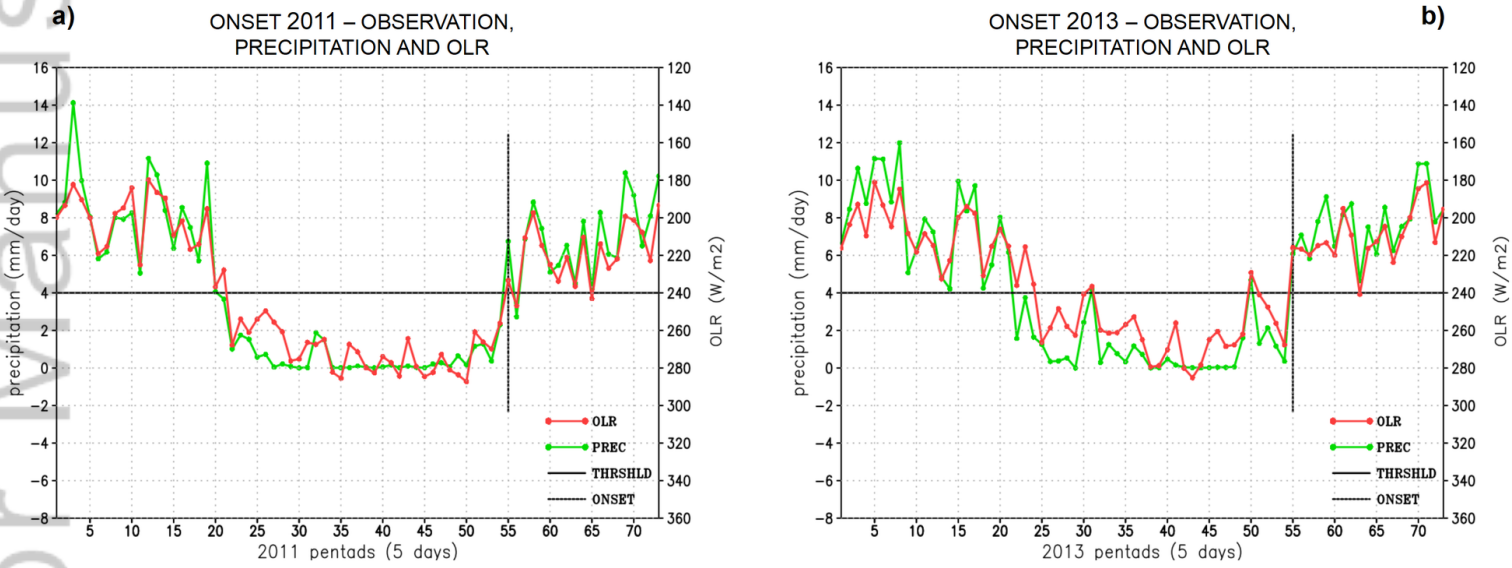

Dragan_Latinovic_figure_5.tif

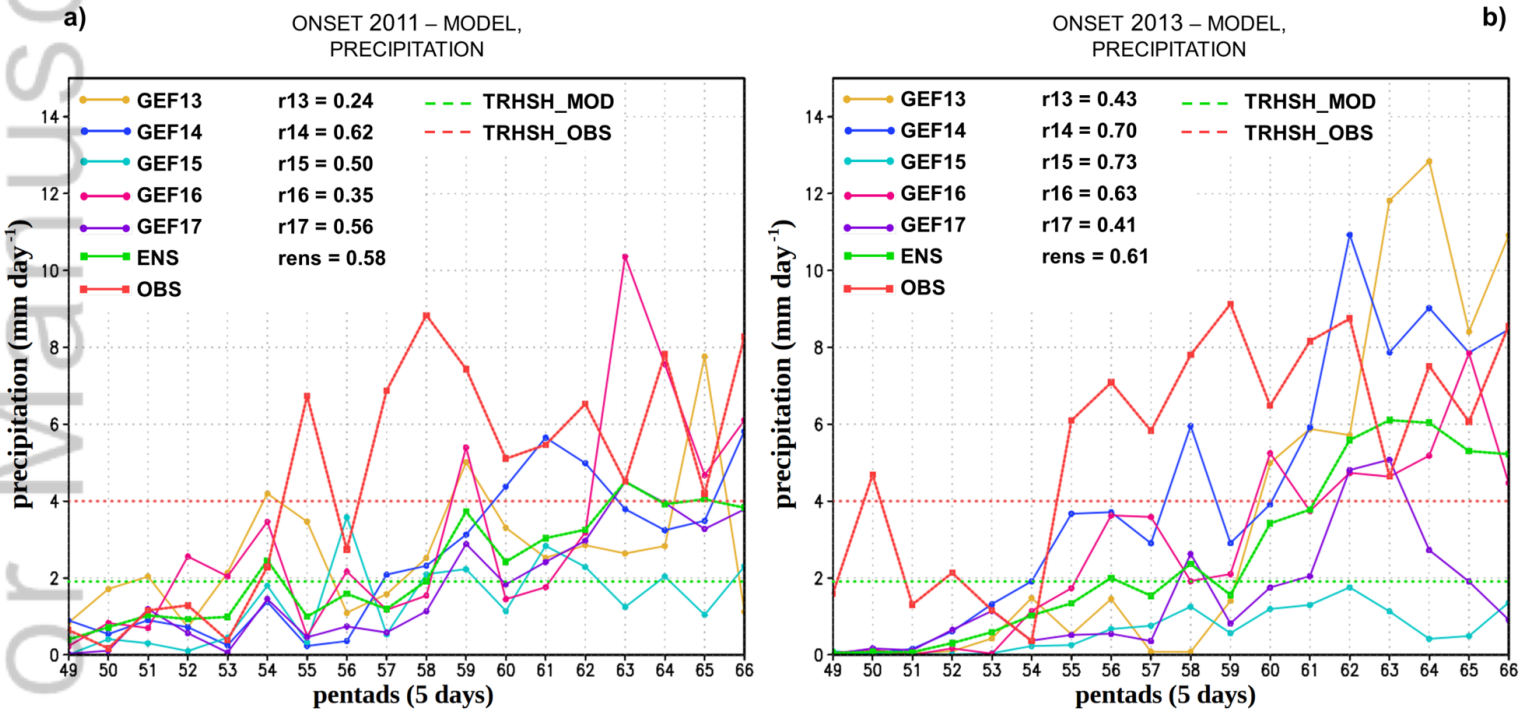

Dragan_Latinovic_figure_6_new.tif

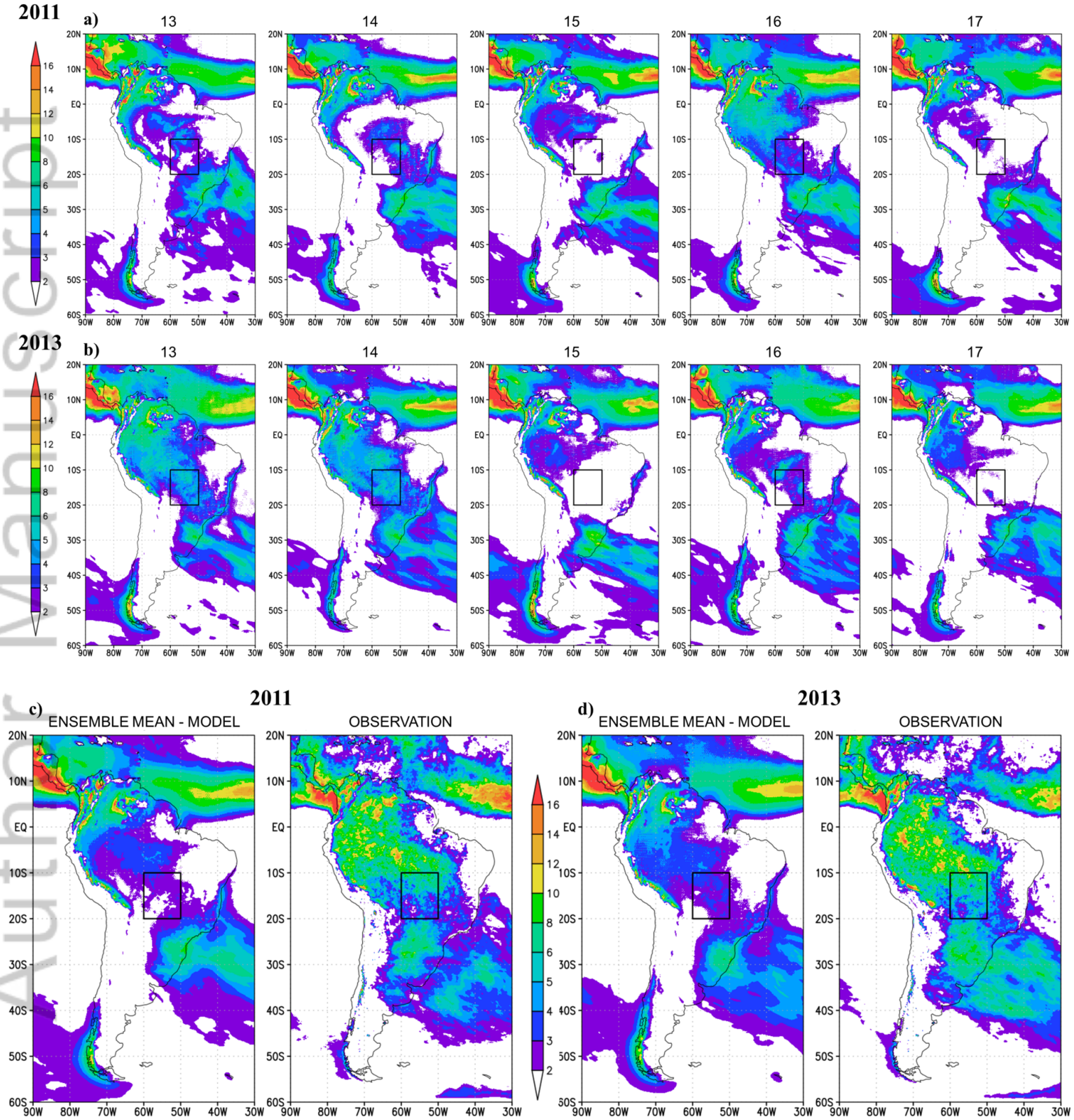

Dragan_Latinovic_figure_7.tif

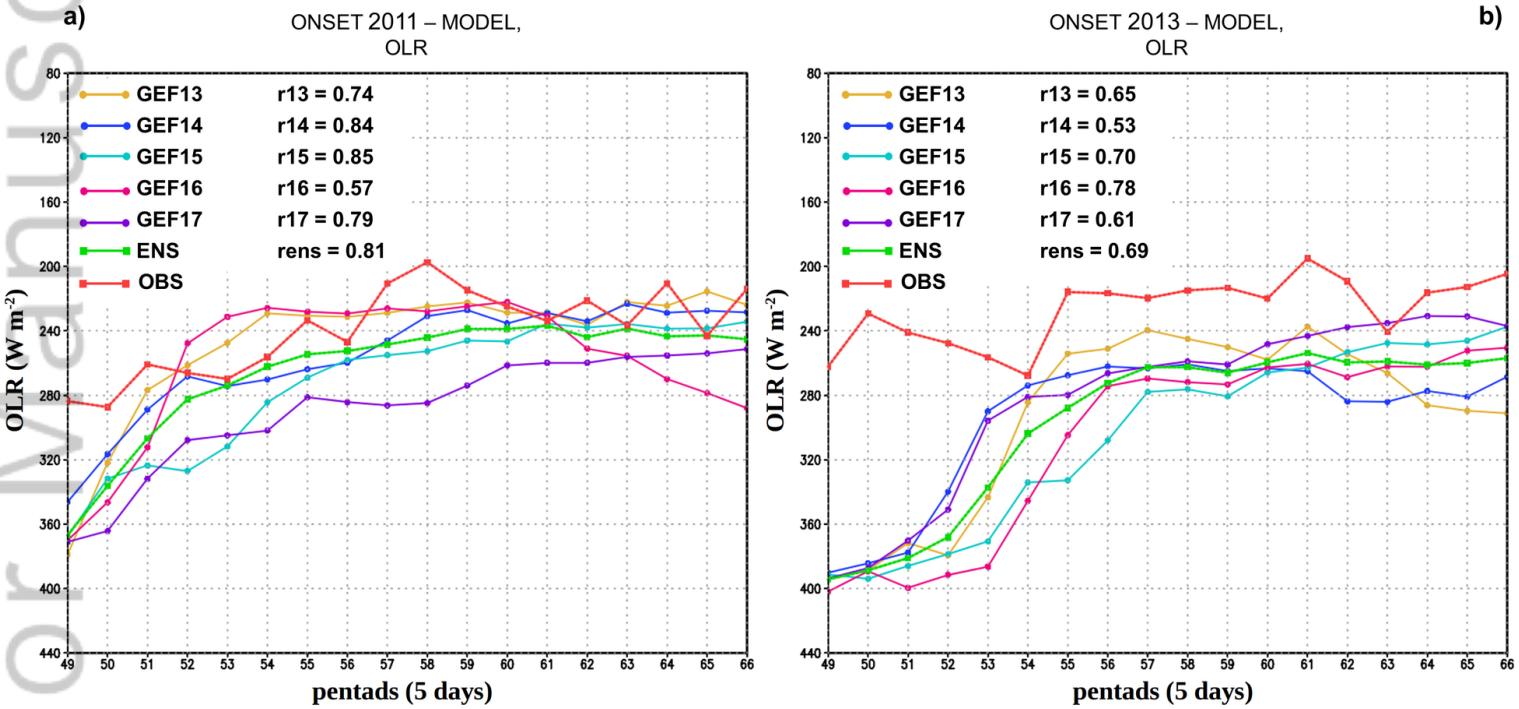

Dragan_Latinovic_figure_8.TIF

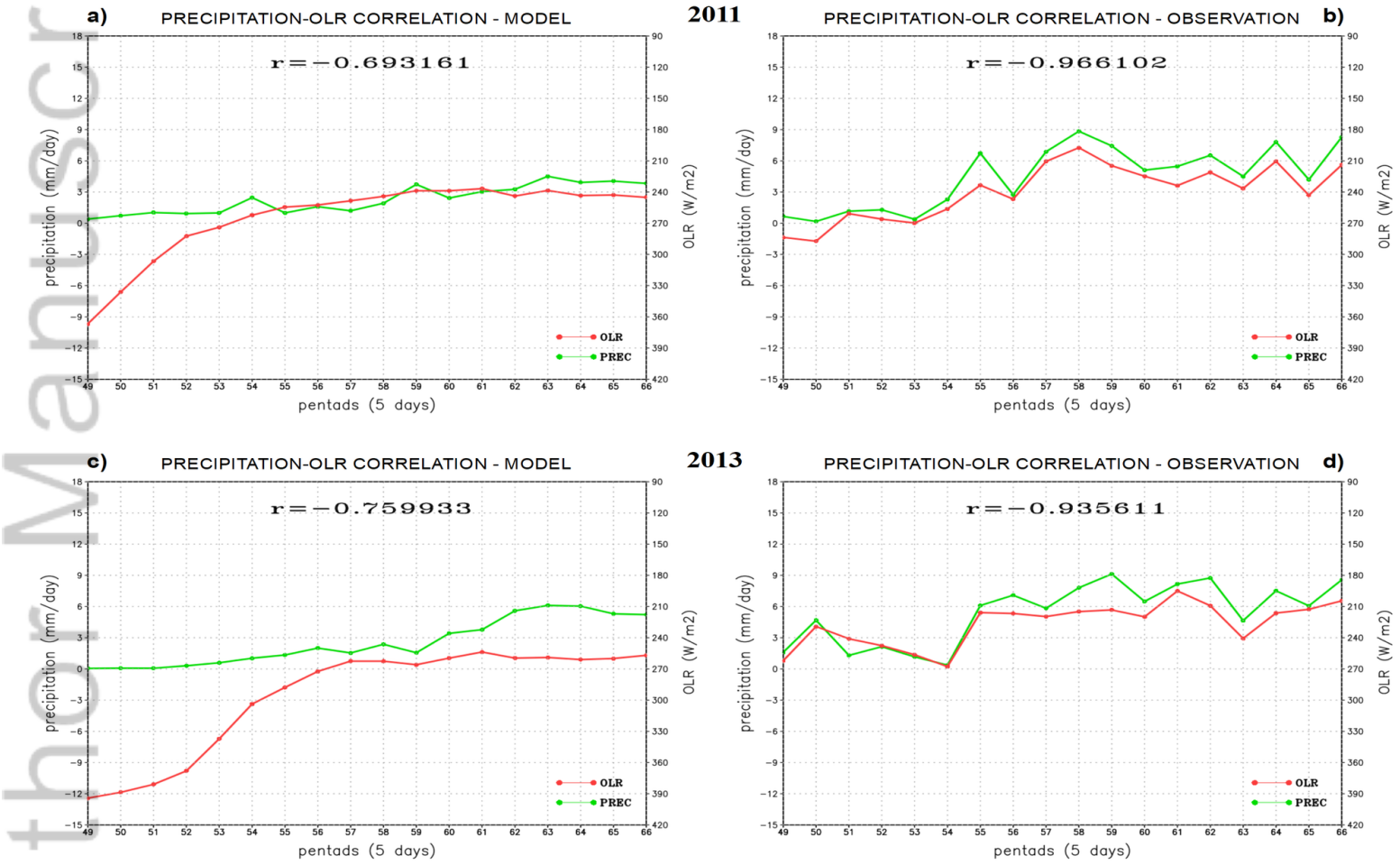

Dragan_Latinovic_figure_9.tif

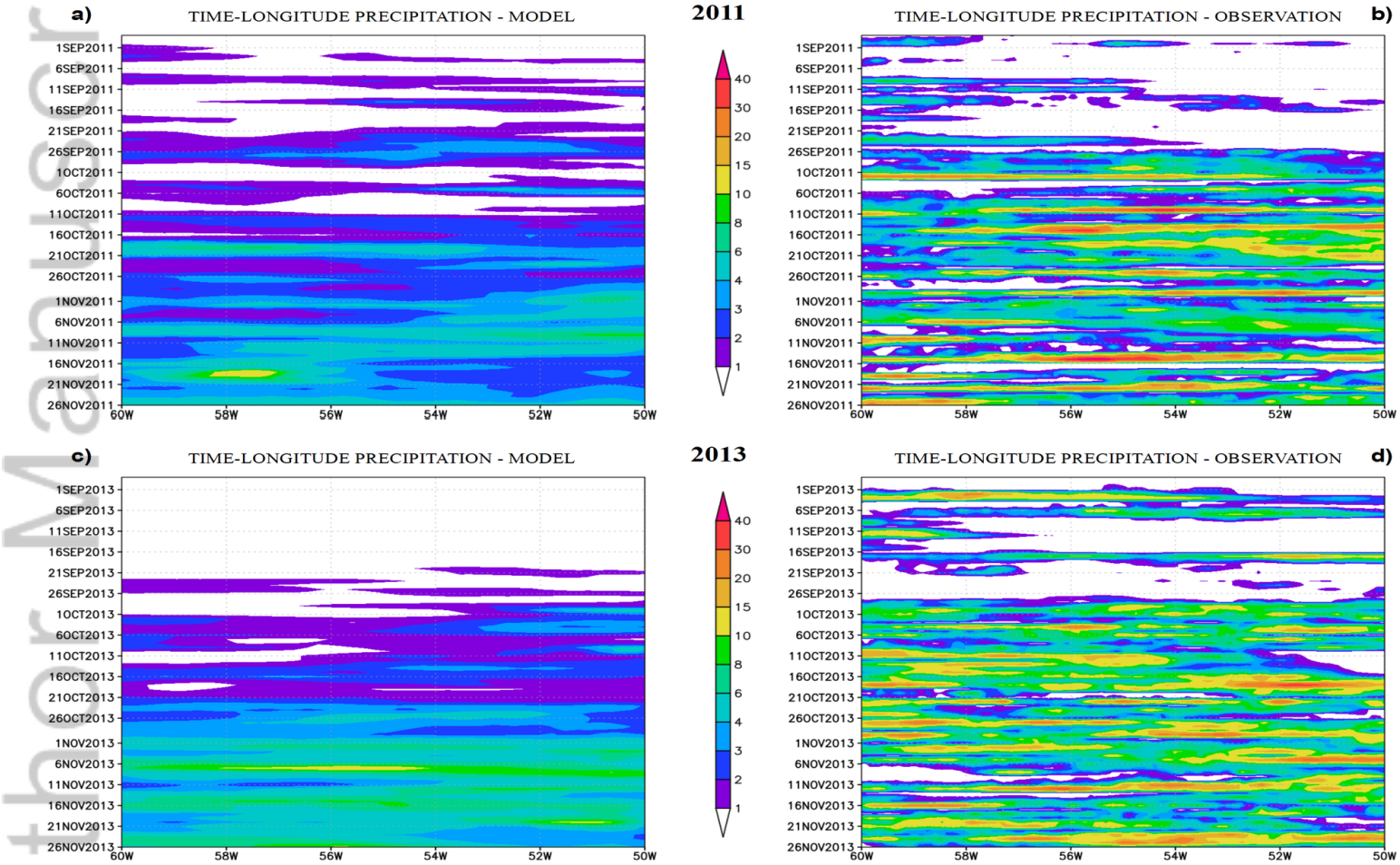

Dragan_Latinovic_figure_10.tif

Seasonal climate and the onset of the rainy season in Western-Central Brazil simulated by Global Eta Framework model

Dragan Latinovi *, Sin Chan Chou, Miodrag Ran i , Gustavo Sueiro Medeiros, André de Arruda Lyra

South American Monsoon System defines the pattern of precipitation in tropical South America. Western-Central Brazil (WCB) region is characterized by remarkable seasonality in annual precipitation and contrast between the summer and winter precipitation patterns. Global Eta Framework (GEF), a global atmospheric model at 25 km horizontal resolution, based on cubed-sphere topology and using regional Eta model infrastructure simulated successfully transition from dry to wet season in WCB region in an ensemble seasonal integration.

Pentad	Dates	Pentad	Dates
49	29 Aug. - 2 Sep.	58	13-17 October
50	3-7 September	59	18-22 October
51	8-12 September	60	23-27 October
52	13-17 September	61	28 Oct. - 1 Nov.
53	18-22 September	62	2-6 November
54	23-27 September	63	7-11 November
55	28 Sep. - 2 Oct.	64	12-16 November
56	3-7 October	65	17-21 November
57	8-12 October	66	22-26 November

Table 1: Pentad numbers and corresponding dates for the pentads 49-66.

variables / trimester	200-hPa wind (m s^{-1})	500-hPa geopotential height (hPa)	850-hPa temperature (°C)	850-hPa wind (m s^{-1})	MSLP (hPa)	precipitation (mm day^{-1})
SON 2011	**0.89**	**0.99**	**0.98**	**0.86**	**0.89**	**0.64**
SON 2013	**0.88**	**0.99**	**0.98**	**0.85**	**0.88**	**0.64**

Table 2: Spatial correlations between mean global simulations and CMORPH observations for precipitation (mm day^{-1}) and the NCEP reanalysis for the remaining variables entered, for SON of 2011 and 2013.